

Performance of the MORA Apparatus for Testing Time-Reversal Invariance in Nuclear Beta Decay

N. Goyal,^{1,*} A. Singh,^{1,†} S. Daumas-Tschopp,² L. M. Motilla Martinez,^{1,3} G. Ban,² V. Bosquet,² J. F. Cam,² P. Chauveau,¹ S. Chinthakayala,^{1,3} G. Frémont,¹ R.P. De Groote,⁴ F. de Oliveira Santos,¹ T. Eronen,³ A. Falkowski,⁵ X. Fléchar,² Z. Ge,³ M. González-Alonso,⁶ H. Guérin,¹ L. Hayen,² A. Jaries,³ M. Jbayli,¹ A. Jokinen,³ A. Kankainen,³ B. Kootte,³ R. Kronholm,³ N. Lecesne,¹ Y. Merrer,² V. Morel,¹ M. Mougeot,³ G. Neyens,⁴ J. Perronnel,² M. Reponen,³ A. Raggio,³ S. Rinta-Antila,³ A. Rodriguez – Sanchez,⁶ N. Severijns,⁴ J. C. Thomas,¹ C. Vandamme,² S. Vanlangendonk,⁴ V. Virtanen,³ E. Liénard,² I. D. Moore,³ and P. Delahaye¹

¹*GANIL, CEA/DRF - CNRS/IN2P3, Bd H. Becquerel, 14076 Caen, France*

²*Université de Caen Normandie, ENSICAEN, CNRS/IN2P3, LPC Caen UMR6534, 14050 Caen, France*

³*University of Jyväskylä, Department of Physics, Accelerator Laboratory,
P.O. Box 35(YFL) FI-40014 University of Jyväskylä, Finland*

⁴*Instituut voor Kern- en Stralingsfysica, KU Leuven, B-3001 Leuven, Belgium*

⁵*IJCLab, 15 Rue Georges Clemenceau, 91400 Orsay, France*

⁶*IFIC, Universitat de València - CSIC, 46980 Paterna, Spain*

(Dated: April 25, 2025)

The MORA experimental setup is designed to measure the triple-correlation D parameter in nuclear beta decay. The D coefficient is sensitive to possible violations of time-reversal invariance. The experimental configuration consists of a transparent Paul trap surrounded by a detection setup with alternating β and recoil-ion detectors. The octagonal symmetry of the detection setup optimizes the sensitivity of positron-recoil-ion coincidence rates to the D correlation, while reducing systematic effects. MORA utilizes an innovative in-trap laser polarization technique. The design and performance of the ion trap, associated beamline elements, lasers and β and recoil-ion detectors, are presented. Recent progress towards the polarization proof-of-principle is described.

I. INTRODUCTION

The Standard Model (SM) of particle physics currently provides the most compelling description of the fundamental interactions between elementary particles. Despite its success, several profound questions remain unanswered. Among those, the SM requires at least 19 arbitrary parameters, the nature of dark energy and dark matter remains unknown, and the origin for the imbalance between matter and antimatter in the universe is still unexplained. A promising avenue for probing New Physics (NP) beyond the Standard Model is through precision measurements in nuclear β decay.

The study of β -decay processes provides a unique laboratory for scrutinizing the weak interaction, one of the four fundamental forces, with unparalleled precision. Historically, the investigation of β decay has led to critical developments in our understanding of weak interactions, from the discovery of parity violation to the formulation of the $V-A$ theory. Recent advances in experimental techniques and detector technologies have significantly enhanced the precision with which β decay parameters can be measured. These advancements open new windows to search for subtle deviations from the predictions of the SM, which may indicate the presence of NP. As such, β decay experiments offer a complementary approach to experiments which directly probe energy scales of NP

through particle collisions at high energies. The complementarity and interplay of these approaches are now very well established thanks to modern Effective Field Theories. With sensitivities reaching the $\sim 10^{-3}$ level on traces of non-standard Wilson coefficients in the effective Hamiltonian of this low-energy process, constraints on interactions involving new particles beyond the TeV regime, such as Leptoquarks or right-handed W bosons, can compete with limits obtained at the Large Hadron Collider (LHC) [1–3].

The Matters Origin from RadioActivity (MORA) project searches for NP by studying the D correlation in nuclear β decay, which occurs in mixed Fermi and Gamow-Teller transitions of spin polarized nuclei [4]. The D correlation is a triple correlation between the spin of the decaying nucleus, the momentum of the emitted electron or positron, and the momentum of the emitted neutrino. It is particularly interesting because it is sensitive to time-reversal symmetry violation, not only in yet unobserved scalar and tensor currents, but also in well-established V, A currents. Any observed T-violating effects are a smoking gun for NP and provide insight into new CP-violation mechanisms, which are necessary to explain the baryon asymmetry in the universe [5].

The particular case of the sensitivity of D to NP was recently reviewed by coauthors of this article [6]. While the search for NP in the framework of specific albeit popular NP Models is constrained to the 10^{-5} level by Electric Dipole Moments (EDMs), pion decay and the LHC, a manifestation of CP violation at the 10^{-4} level is not excluded by a direct measurement of D . The most con-

* Also at Synchrotron SOLEIL, 91190 Saint-Aubin, France

† Also at IRSN/LMRE, Rue du Belvédère – 91400 Orsay, France

straining measurement to date has been obtained from neutron decay by the emiT experiment: $D_n < 2 \cdot 10^{-4}$ [7, 8]. The MORA experimental program is therefore organized in two phases: the first phase, conducted at the Ion Guide Isotope Separation On-Line (IGISOL) facility [9] at the University of Jyväskylä, Finland, aims to obtain a sensitivity to a non-zero D correlation competitive with the emiT experiment; the second phase, carried out at GANIL in the future DESIR facility, targets a sensitivity of the order of $\sim 10^{-5}$ [4], sufficient to start probing NP from specific models.

To acquire the required statistics for the ambitious goals of the experiment, MORA makes use of an innovative technique, combining the high efficiencies of ion trapping and laser polarization. We present here the current status of the MORA experimental setup at IGISOL. The following sections describe successively the experimental setup, the commissioning of the beamline, the ion trap and its performances, and the characterization of the detection setup. The calculation of the sensitivity factor on D , that depends on the phase space selected by the detection setup of MORA (parameter δ introduced in Eq. 5 of ref. [4]), and the evaluation of possible systematic effects are then presented. The last section concludes on the results of the latest experimental progress to demonstrate the laser polarization technique.

II. THE MORA APPARATUS

The MORA experimental setup is a novel apparatus that has been designed and built to store and polarize radioactive ions and observe their subsequent decay. With this apparatus, $^{23}\text{Mg}^+$ and $^{39}\text{Ca}^+$ ions are the most promising candidates for the D correlation measurement [4]. The whole MORA setup consists of an injection beam line, a transparent Paul trap and a detection setup. The injection beam line decelerates the ions delivered by the IGISOL RFQ cooler buncher to allow their efficient capture in the transparent Paul trap [10, 11]. The latter permits the in-situ polarization of the ion cloud. The detection setup surrounding the trap is optimized to maximize solid-angle coverage for positrons and recoil ions emitted after β decay.

A. MORA at IGISOL

Figure 1 shows the integration of the MORA apparatus within the IGISOL facility [9]. At IGISOL, low-energy radioactive ion beams are produced via light-particle (p, d, ^3He , ^4He) and heavy-ion induced reactions in a gas cell. These reactions include fission, used in the majority of experiments, as well as transfer or fusion-evaporation reactions, of particular interest for MORA. Because of charge recombination with the gas and impurities in the cell, most of the reaction products stopped in the gas are eventually delivered from the cell as singly charged

ions. A sextupole ion guide [12] permits their collection as a beam before acceleration to 30 keV, and subsequent mass separation thanks to a dipole magnet. In the IGISOL hall, the radioactive beams can be cooled by the IGISOL RFQ cooler in a High Voltage (HV) cage, which has been recently upgraded with a minibuncher to enable bunching of ions with a time spread < 100 ns [13]. The minibuncher has been developed for the Multi-Reflection Time-of-Flight Mass Spectrometer (MR-ToF-MS) of IGISOL, allowing for a fast separation of isobars and mass measurement of short-lived isotopes. Ions are transported to different setups at an energy of ~ 2 keV (e.g. to the JYFLTRAP Penning trap [14] or RAPTOR [15]).

For practical reasons, including protecting fragile electronics and detection setup from sparks, and avoiding possible sources of noise related to the delicate definition of reference potentials, the MORA apparatus is standing just beyond the HV cage downstream from the MR-ToF-MS. MORA therefore requires a particular beam manipulation for the decelerating and trapping of ions to sub-eV energies, as is detailed in the next section. So far the beam production and manipulation efforts for MORA have been limited to $^{23}\text{Mg}^+$ ions, as those only require one laser frequency for their polarization, compared to two for $^{39}\text{Ca}^+$ ions. The laser light required for the polarization of $^{23}\text{Mg}^+$ ions is prepared on a laser table neighbouring the MORA setup, also used for RAPTOR campaigns. Circular polarization of the laser beam and control over its handedness required for MORA is done on a small platform (80 cm x 50 cm) attached to the trap chamber of MORA (see section IID). The production of $^{23}\text{Mg}^+$ ions in the IGISOL gas cell is described in section IV.

B. MORA beam line

To enable efficient deceleration and capture of ions in the trap of MORA, the injection beam line has been originally designed using SIMION [16] simulations. The mechanical components of MORA, i.e. ion optics, electrodes of the ion trap, trap and injection chambers, and the detection frames have been conceived and manufactured in-house, by the LPC Caen workshop, to enable an alignment precision of ≤ 100 μm . Special care was particularly taken for the support of detectors surrounding the trap described in section IIE. The injection beam line is shown in Fig. 2, together with the ion trap. It contains two Pulsed Drift Tubes (PDTs) for the deceleration of ions, ion optics for steering and focusing, and different diagnostics for ion counting and laser alignment.

1. Deceleration of ions

The PDTs enable the progressive deceleration of the bunches delivered by the minibuncher for their efficient

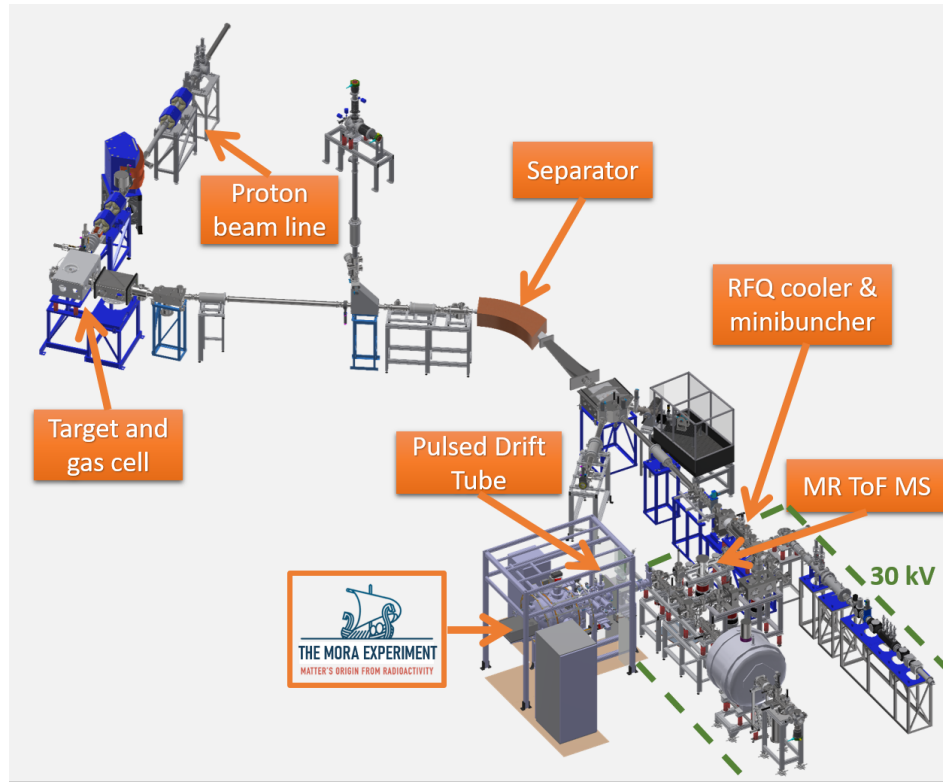


FIG. 1: Sketch of the production system and IGISOL hall featuring the different components important to MORA. The dashed line shows the footprint of the high voltage cage.

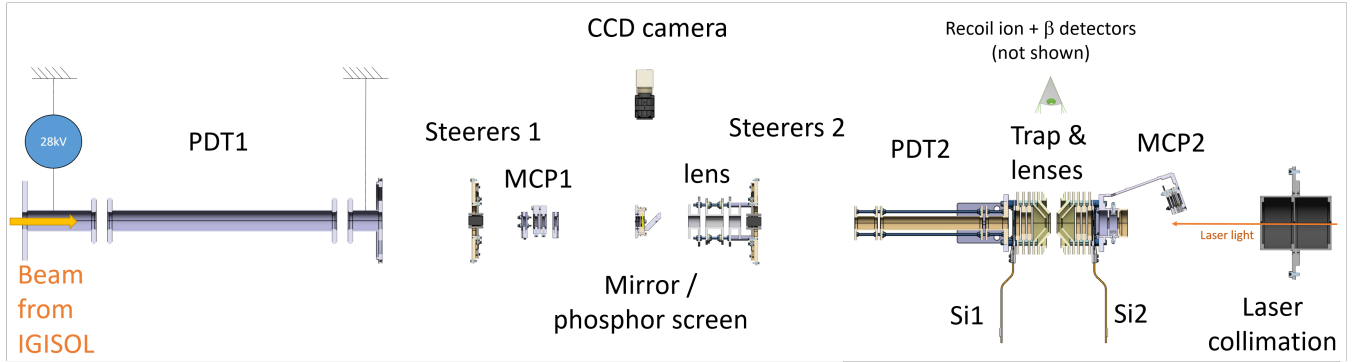


FIG. 2: Simplified view of the injection line, trap and ion counting systems.

capture in the trap. They consist of a central cylindrical electrode framed by two shorter ones at the reference potential of the beam line. The central electrode of PDT1 is half contained in the HV cage of IGISOL and half in the grounded part of the injection beam line (the HV and injection beam lines are connected by a ceramic break surrounding the PDT central electrode). The upstream reference potential is therefore about +28 kV to ground (reference potential of the HV cage), while the downstream one is ground. For PDT2 the reference potential is simply ground on both sides. The length of the central electrode for both PDTs has been chosen in order to accommodate with a safety margin (factor ~ 3) the spa-

tial distribution of $^{23}\text{Mg}^+$ ion bunches of 1 μs : 40 cm for PDT1, for accepting bunches of 2 keV, and 18 cm for PDT2, for accepting 150 eV bunches. The principle of the deceleration of ions in the PDTs is illustrated in Fig. 4. When the ion bunch is crossing the center of the drift tube, the voltage of the tube, playing here the role of a Faraday cage, is switched from a positive value to a negative one. The ion's motion is therefore not affected by the sudden change of potential until it reaches the end of the drift tube, where it is eventually decelerated. The balancing of the positive and negative voltages enables control on beam focussing, similar to that obtained by tuning the RF phase of accelerating cavities.

PDT1 reduces the kinetic energy of ions crossing the HV cage towards the injection beam line by ~ 500 eV. Its potential is switched from approximately 28 kV (the reference potential of the HV cage) to -500 V relative to ground, using a 30 kV Behlke switch from the HTS series, together with Spellman +30 kV / -2 kV power supplies. The quality of this switching is critical for MORA, as it must avoid generating energy dispersion or shifts larger than ~ 10 eV, which would reduce the efficiency of the ion capture in the trap. While achieving a sufficiently short switching time - less than 1 μ s compared to the ions' transit time of $\simeq 3$ μ s - has never been an issue, maintaining voltage stability before and after switching, when ions enter or exit the PDT, has proven to be a challenging task. Multiple sources of large, rapid fluctuations (μ s/ms), as well as longer-term drifts and variations (min/h), had to be identified and addressed. The key measures taken to eliminate these sources are listed below:

- The initial configuration of our switch included two HTS30 modules from Behlke in cascade to allow for a possible usage of the switch with up to 60 kV. The switching circuit was simplified, in order to avoid problems of desynchronisation of the HTS modules, as indicated by Behlke. The final version of the switching circuit is shown in Fig. 3.
- The impedances of this circuit had to be carefully selected so as to produce stable pulsing. In particular the rather small 5 M Ω resistor was chosen to reduce the dependence on the positive voltage to possible impedance fluctuations of the HTS switch. The 1 k Ω resistor was found suitable for optimizing trapping efficiencies. With such a resistor a fast switching of ~ 200 ns could be obtained, while reducing voltage oscillations after switching.
- The resistors and connections to the positive and switch output were covered with kapton to avoid micro-sparks. These microsparks, observed experimentally, were inducing erratic energy variations, up to 100 eV.
- The logical signal triggering the switch and the +24V switch supply had to be shielded against the EM noise generated by the switching to avoid unwanted retriggering or switch malfunction.
- The electrical connection of the positive HV supply to the 5 M Ω had to be redone several times to ensure firm contact, and prevent microsparks during the switch operation.
- Grounding loops between the HV power supplies and the switch circuit generated unwanted noise and had to be eliminated.

The recent elimination of all the sources of instability resulted in a drastic improvement in the trapping efficiencies, presented in section II C).

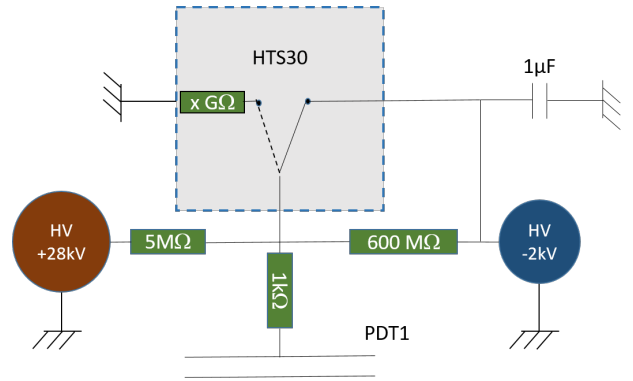


FIG. 3: Sketch of the switching circuit. The HTS30 switch from Behlke has an impedance of several G Ω to ground.

PDT2 requires the switching of more modest voltages. It is therefore less critical and has always been well-functioning. PDT2 decelerates ions further down to 150 eV, just before the ion trap. PDT2 voltages are produced by a 2kV switch from CGC, fed by two ISEG +1.5kV and -0.5kV power supplies. The switching is very rapid (~ 10 ns) and produces negligible fluctuations after 1 μ s, when ions exit from the PDT2.

The injection beam line also includes beam optics to align and focus the beam through the PDTs; two sets of x and y steerers formed of four electrodes are placed just after PDT1 and just before PDT2. An Einzel lens is placed in the middle of the steerers to focus the beam properly before entering PDT2.

2. Diagnostics for the deceleration of ions

Three sets of attenuators, each consisting of electroformed meshes with 10% transmission and mounted on pneumatic actuators, help regulate the ion flux. This enables ion-by-ion detection using a removable Micro-Channel Plate detector (MCP1) and associated phosphor screen, also mounted on an actuator (Fig. 5). The phosphor screen can be used to get a qualitative display of the beam shape and position. It is read by a CCD camera wrapped with a piece of black fabric to get rid of external light. Alternatively, the MCP1 and phosphor screen can be replaced by a mirror to monitor the alignment of the laser beam used to polarize the ion cloud (see section IID).

MCP1 also features a set of two meshes: one at ground potential with a 90% transmission efficiency and another one at a variable potential, with an additional 10% transmission factor. This retardation potential can be used to measure the energy of the beam with an energy resolution of a few eV, to be compared to an expected dispersion of ~ 10 eV after the minibuncher, more or less matching the acceptance of the trap of MORA. With all the sets of attenuation meshes, up to a few 10^5 ions per bunch can

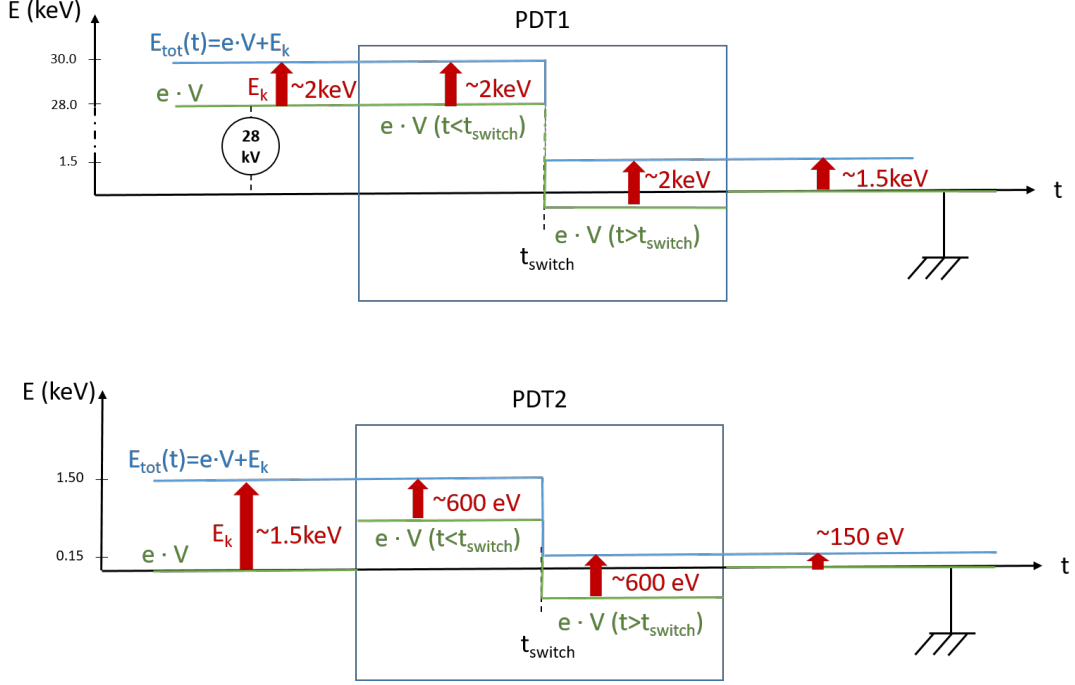


FIG. 4: Principle of deceleration in PDT1 and PDT2. The total, kinetic and potential energies (resp. E_{tot} , E_k and $e \cdot V$) of ions passing through the PDTs are plotted as a function of their time-of-flight t .

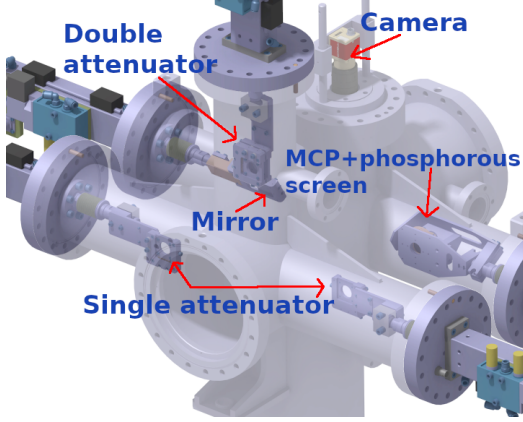


FIG. 5: Diagnostics of the injection beamline displayed on the user interface.

safely be detected by such an ion counting system. The MCP1 calibration is done using fast cycles and comparing the ion counting rate with measurement of currents on FCs situated in the HV cage. Time-of-flight of ions are recorded and analyzed thanks to the FASTER acquisition [17], developed by LPC Caen, and also used for the detection system described in section II E.

C. Ion trap

The trap of MORA is situated at the end of the injection beam line and in the center of the detection setup. Its open geometry has been adapted from LPCTrap [11], and further optimized by simulations to enlarge the volume in which the potential is harmonic [10]. As a result, an increase of 27% of the radial acceptance and an increase of 50% of the ion capacity is expected, for the same RF voltage and for a comparable characteristic dimension, usually referred to as r_0 [18].

1. Trap characteristics

The trap is composed of six independent ring-shaped electrodes labeled R1 to R6 in Fig. 6. R3 and R4 are pulsed electrodes used for respectively ejecting and injecting ions from / into the trap. During trapping, these electrodes are grounded, and the RF voltage is applied on R1 and R2. Using standard notations [18], R1 and R2 act as end caps, while R3 and R4 serves as the ring electrode. R5 and R6 are correcting electrodes, always at ground. This configuration minimizes RF disturbances affecting recoil ions produced by β decay as they travel to the detectors. The trap is enclosed by two sets of einzel lenses, which optimize the focus of the ion bunch for injection and extraction. These einzel lenses are switched off during trapping to minimize their disturbance on the

RF field.

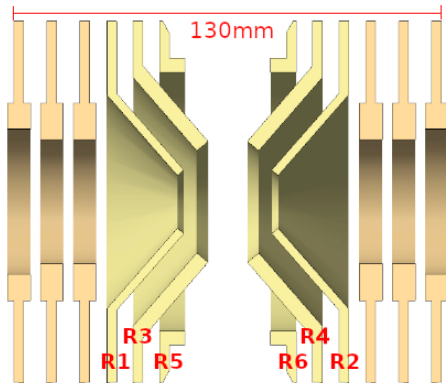


FIG. 6: Schematic view of the MORA trap displayed on the slow control user interface.

The RF is generated by a generator from Keysight and amplified by an amplifier from Falco Systems, capable of delivering a nearly perfect sine wave of ~ 200 V peak-to-peak on a wide range of frequencies, from a few 100 kHz to a few MHz.

A buffer gas of ^4He is injected at a pressure of approximately 10^{-5} mbar during trapping for ion cooling and reducing the Doppler effect for an efficient laser polarization.

2. Diagnostics for ion trapping

On the side opposite the injection line, a small electrostatic deflector enables the off-axis detection and counting of the ions of the cloud on MCP2. MCP2 is very similar to MCP1. It is also equipped with a retardation mesh to measure the energy dispersion of decelerated ions passing through the ion trap. This diagnostic is used for the optimization of the PDT2 and R4 stopping voltages applied to capture the ions into the trap. Ion counting enables the determination of the performances of the trap, in terms of efficiency and ion trapping lifetime. It is also used on-line for monitoring the number of trapped ions after each cycle of injection - trapping - extraction. So far, cycles of 11 s, corresponding to ~ 1 half-life of ^{23}Mg and consisting of 6 s of trapping and 5 s of background measurement were used. During the on-line operation, all attenuation mesh in the injection beam line are removed (Fig. 5). The attenuation factor is therefore limited to that of the mesh used for the energy measurement, directly attached to MCP2 (factor of ~ 10). With typical trapped ion numbers of a few 10^4 , the extraction of the ion cloud results in a few E3 ions reaching MCP2 within 100 ns. The number of trapped ions is therefore not measured using event-by-event detection, but roughly estimated by integrating cycle per

cycle the total charge deposited and amplified by MCP2. With such technique, the precision on the ion number is rather modest, of the order of 50%.

3. Performances: Trapping efficiency and trapping lifetime

Preliminary results obtained with a stable alkali ion source delivering a 2 keV $^{23}\text{Na}^+$ ion beam at LPC Caen and reported in [19] have generally improved in the past two years at the University of Jyväskylä, thanks to the use of a better adapted RF system, and an improved understanding of the key parameters governing capture and ion trapping. Among other findings, it was discovered that starting the flow of 6.0-grade He gas through a zeolite filter to the trap chamber 24 hours before operation resulted in an enhanced ion trapping lifetime. We therefore only show here the latest results. At the University of Jyväskylä, trapping optimizations are usually performed with stable $^{23}\text{Na}^+$ ions delivered from a stable ion source prior to the actual data taking with proton beam on target. One particular challenge is the deceleration in PDT1, which requires that the positive and negative high voltages established by the switch are stable within a few volts, when ions are entering or exiting the drift tube. In the initial experiments, this condition was not fulfilled. Careful work was therefore carried out to address all sources of instability, as detailed in Section II B. Once these sources were identified and eliminated, the trapping efficiencies reached stable values comprised between 30 and 40%, without retuning required for over 24 hours. The trapping half-life of ions was measured with and without He cooling by counting the number of ions ejected to MCP2 after trapping times ranging between a fraction of a second and 10 seconds (see Fig. 7). While it is limited to values of the order of 3 s without cooling, it can exceed 10 s with ion cooling. For the latter case, the evaporation of the ion cloud, as monitored during the trapping phase with the recoil ion detectors (see section II E 3), shown in Fig. 8, provides an indirect estimate. The evaporation rates are proportional to the trapped ion number, as discussed in Ref. [11]. After thermalization, the rates follow an exponential decay that can be fitted with a reasonable p-value. The thermalization happens faster in the case of ion cooling. An approximate thermalization time of 300 ms is observed when buffer gas cooling is applied, compared to more than 1 s without ion cooling. The trapping half-lives deduced from the fits are 68 ± 10 s and 3.05 ± 0.13 s with and without ion cooling respectively. These indirect estimates are consistent with the direct measurements shown in Fig. 7.

D. Laser polarization

As discussed in [4], a circularly polarized laser beam of 35669.31 cm^{-1} must be generated to excite the D1

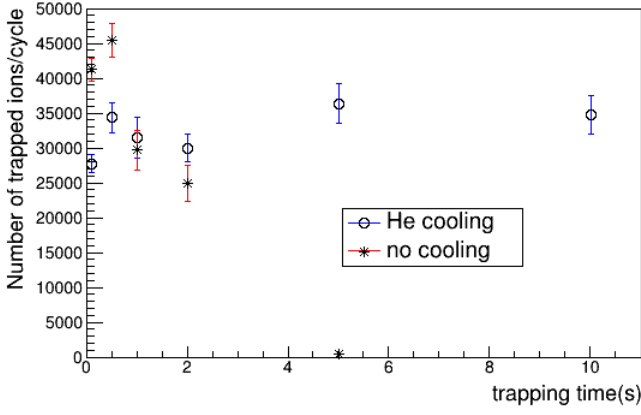


FIG. 7: Number of ions as a function of trapping time, measured with MCP2 with and without He cooling. The statistical errors are inflated by a factor two to take into account variations in the transport efficiencies from the IGISOL minibuncher to the trap and from the trap to MCP2.

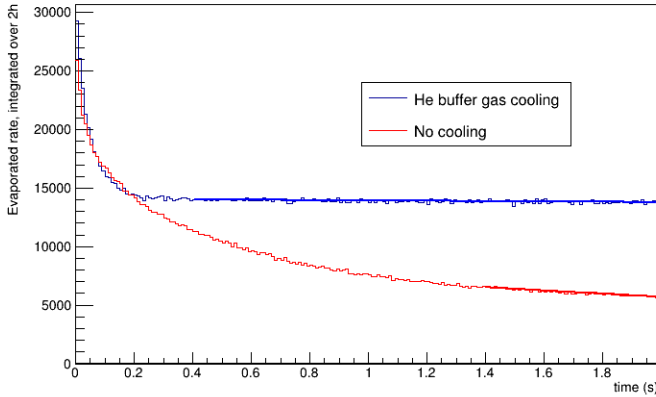


FIG. 8: Rates of evaporation of the $^{23}\text{Na}^+$ cloud as measured with the recoil ion detectors. The lines superimposed on the data are exponential chi-squared fits with p-values of 51% with cooling and 30% without. See text for more details.

hyperfine transition of $^{23}\text{Mg}^+$ ions for their efficient spin orientation. At IGISOL, this is produced by frequency tripling the fundamental laser output of a Ti:Sapphire cavity pumped by a Nd:YAG laser. As shown in Fig. 9, the circular polarization of the laser light is achieved using optics mounted on a small table attached to the MORA trap chamber. A rotatable half-wave plate optimizes the transmission through a Polarizing Beam Splitter cube (PBS) selecting only one linear polarization. A quarter wave plate is then used to obtain circularly polarized light, that is referred by convention to σ^+ in the following. This light enables the polarization of the ion

cloud towards the direction of propagation of the laser (see section IV B). It is optionally followed by a half-wave plate to switch the circular polarization of the laser light, from σ^+ to σ^- . Another PBS is used for diagnostics purposes between each measurement period, to ensure that the powers in the horizontal and vertical polarization components are balanced after the quarter-wave plate.

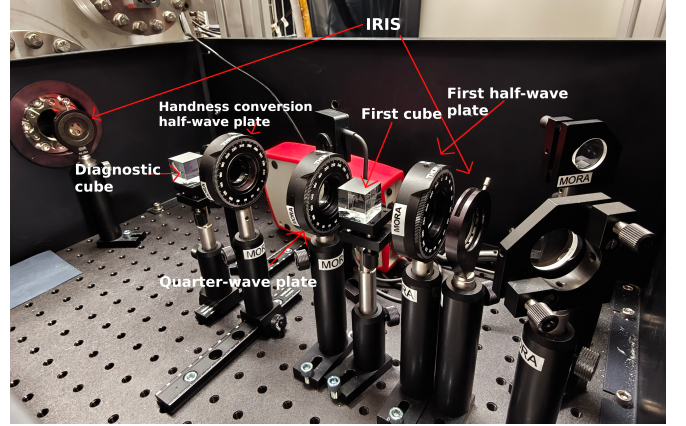


FIG. 9: Photograph of the laser polarization table. The window to the MORA chamber can be seen on the far left.

E. The Detection setup

The positioning of detectors around the trap of MORA enables maximal sensitivity for the measurement of the D correlation parameter [4]. The setup is inspired from the one of the emiT experiment [7, 8]. It alternates β and recoil detectors every 45° in an octagonal arrangement at a distance of approximately 10 cm from the trap center. Given the polarization direction, the D correlation can be inferred from an asymmetry in the number of coincidences recorded at average positron - recoil angles ($\theta_{\beta r}$) of $+45^\circ$, $+135^\circ$ on one hand and -45° , -135° on the other, the sign of θ being defined clockwise with respect to the spin direction, as illustrated in Fig. 10. The asymmetry given by

$$D = \frac{1}{\delta \cdot P} \frac{N_{coinc}^{+45} + N_{coinc}^{+135} - N_{coinc}^{-45} - N_{coinc}^{-135}}{N_{coinc}^{+45} + N_{coinc}^{+135} + N_{coinc}^{-45} + N_{coinc}^{-135}} \quad (1)$$

linearly depends on the product of two sensitivity factors:

- δ , a constant term depending on the detection solid angle and the decay parameters, which can be simulated with % precision with standard Monte Carlo techniques.
- P , the polarization degree, which can be inferred from a β asymmetry measurement in the axis of the Paul trap [4] thanks to 2 Silicon annular detectors (see sections II E 1 and IV B).

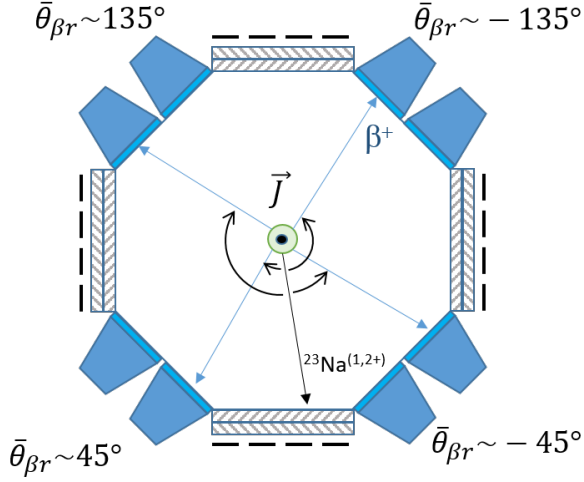


FIG. 10: The D correlation detection setup in the azimuthal plane of the trap. β 's are detected by Phoswich detectors (see section II E 2), while recoil ions are detected by a chevron stack of Micro-Channel Plates (MCPs) followed by a resistive anode (dashed lines; see section II E 3).

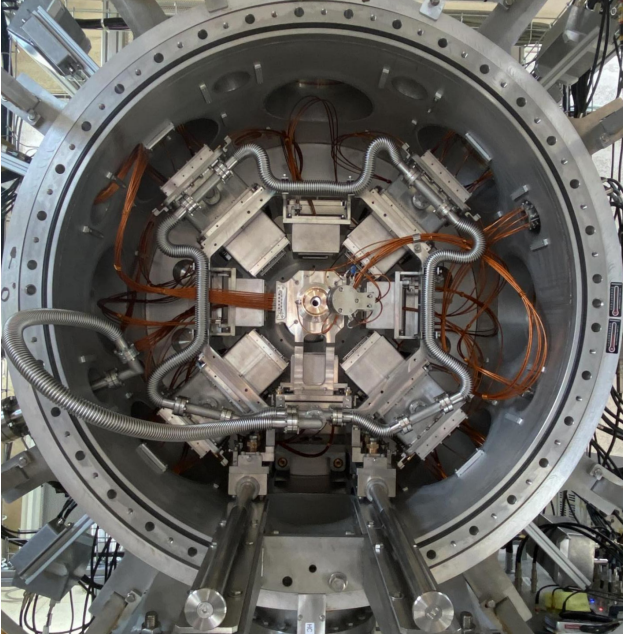


FIG. 11: Photograph of the detection setup around the trap. The trap chamber diameter is about 1m.

In the azimuthal plane of the trap, 4-quadrant scintillation-based phoswich detectors (section II E 2) detect β particles, whereas position sensitive, MCP-based detectors are used for recoil ions (section II E 3). A photograph of the detectors around the trap is shown in Fig. 11. After the β^+ decay of $^{23}\text{Mg}^+$ or $^{39}\text{Ca}^+$ ions, recoils are either neutral or positively charged ions because of the reorganization of the electron cloud (shake-off). In

the case of $^{23}\text{Mg}^+$, on which the first efforts are focused, a shake-off probability yielding 1+ and 2+ charge states of $\sim 26\%$ was estimated [20]. With a maximum energy below 300 eV, the neutral recoils are expected to be detected with modest efficiencies (percent level as generally observed in MCP detectors [21]) compared to the ionized recoils ($\simeq 50\%$, see section II E 3).

During the measurement of the D correlation, the polarization degree is being monitored by the continuous measurement of the β asymmetry along the axis of the trap, thanks to two identical annular Si detectors on opposite sides of the trap (see Fig. 2 and Fig. 1 of ref. [4]). Assuming that Si1 and Si2 detectors have similar efficiencies, and that the activity accumulated over the σ^- and σ^+ laser light illumination periods is similar, we define the equivalent experimental asymmetries

$$A^+ = \frac{N_1^+ - N_2^+}{N_1^+ + N_2^+} \simeq -A^- = -\frac{N_1^- - N_2^-}{N_1^- + N_2^-} \quad (2)$$

and

$$A_1 = \frac{N_1^+ - N_1^-}{N_1^+ + N_1^-} \simeq -A_2 = -\frac{N_2^+ - N_2^-}{N_2^+ + N_2^-} \quad (3)$$

where N_1^+ , N_1^- , N_2^+ , N_2^- represent the number of counts detected in Si1 and Si2, corresponding to laser polarization states σ^+ and σ^- respectively. These asymmetries are proportional to the polarization degree P

$$A^+ \simeq -A^- \simeq A_1 \simeq -A_2 \simeq \alpha \cdot P \quad (4)$$

where α is a constant, which can also be determined to the percent level. The proof-of-principle of the laser polarization was the initial objective of the MORA campaigns at the IGISOL facility. The recent progress is reported in section IV B.

1. Annular Silicon detector

The active surface of the 1 mm thick silicon wafer of the identical Si1 and Si2 detectors consists of two annular rings divided in four sectors (Fig. 12). The inner radius of the smaller ring, of 15 mm, enables the ion injection and extraction, and the passage of the laser beam. The larger ring has an inner radius of 30 mm and an outer radius of 40 mm. The Si wafer is mounted on a ceramic PCB to be compliant with Ultra High Vacuum (UHV) standards in the trap chamber. The Si detectors are covered by an aluminum protection sheet of 100 μm thickness to stop photons from the diffusion or the reflection of the laser light used to polarize the $^{23}\text{Mg}^+$ and $^{39}\text{Ca}^+$ ions.

The Si detectors were first characterized offline with a 3- α source and without their protection cover. During these tests a resolution of 28 – 30 keV was obtained with α -particles of energies ranging from 5 to 5.5 MeV. Characterizations were pursued with a ^{207}Bi source for determining the resolution for β particles with the aluminum

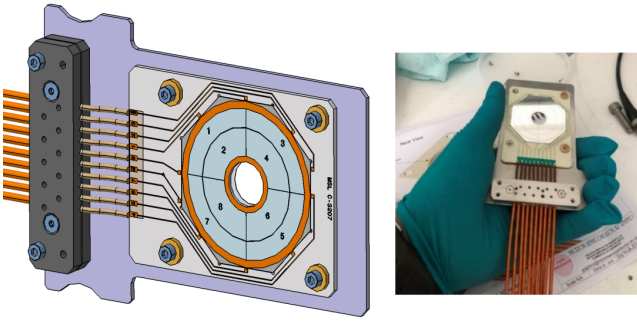


FIG. 12: Sketch and photograph of the Si detectors.

cover. Mesytech MPR-16-L preamplifiers were chosen for their performance for low-energy electrons. Figure 13 shows an example of recorded spectrum. An average energy resolution of 20 keV FWHM is obtained for the 975 keV and 1049 keV conversion electron peaks, as well as an energy shift of 40 keV, consistent with the simulation and calculation of energy straggling and loss in the aluminum protection cover. A detection threshold of 50 keV has been obtained for all channels after carefully reducing EM noise. In total 3 identical Si detectors were produced on demand by MICRON for MORA. Each detector was individually tested. The two best-performing detectors were selected for installation on the trap axis.

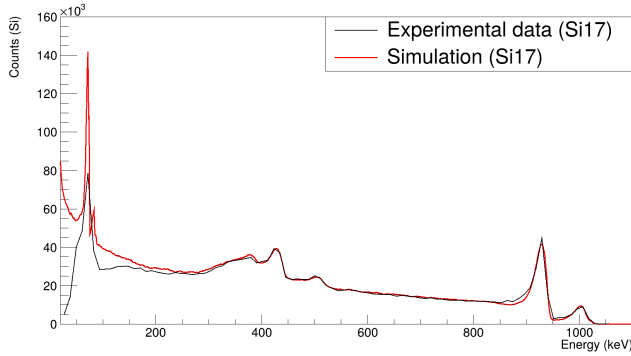


FIG. 13: Example of ^{207}Bi decay spectrum as measured by one sector of the Si detectors compared to PENELOPE simulations.

2. Phoswich detectors

Each of the four phoswich quadrants features two plastic scintillators stacked on top of each other and connected to the same photomultiplier tube (Fig. 14). The first scintillator, only 0.5 mm thick (Scionix EJ-204) has a fast scintillation time constant ($\tau = 1.8$ ns) whereas the second, 5 cm thick scintillator (Scionix EJ-240) has a much larger time constant ($\tau = 285$ ns). The very different response times of the two detectors enables to

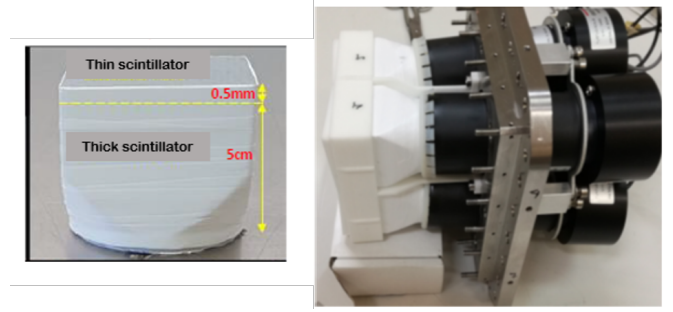


FIG. 14: Phoswich detector. Left pane: the thin and thick scintillators. Right pane: the 4-quadrant assembly.

discriminate between γ -particles and positrons by simple pulse-shape analysis as illustrated in Fig. 15. As the γ -particles have a high interaction probability in the thick scintillator but a negligible one in the thin scintillator they are characterized by a small fast component. This is in contrast to positrons, which will always deposit some of their energy in the thin scintillator. On this figure, Q_{fast} is the charge delivered by the photomultiplier tube and integrated over the first 16 ns of the signal, while Q_{slow} is integrated on a window starting just after Q_{fast} and stopping after 1.5 μs .

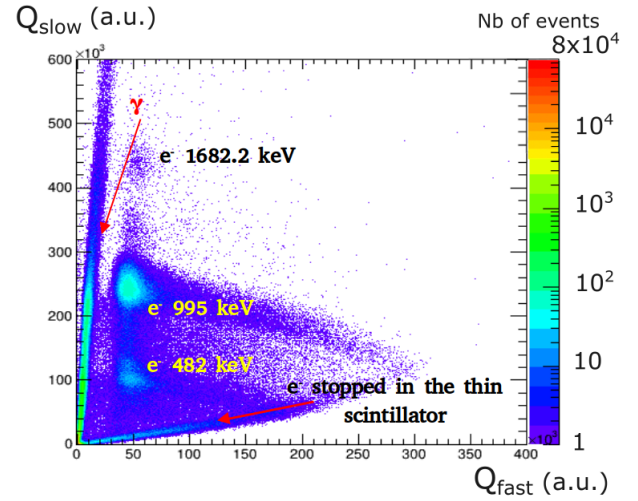


FIG. 15: Example of Q_{slow} vs Q_{fast} spectrum measured with the phoswich detectors, when using a ^{207}Bi calibration source. The Q_{slow} and Q_{fast} charges are displayed as integrated by the FASTER acquisition, in arbitrary units.

The Phoswich detectors were initially assembled and tested at LPC Caen. Resolutions of the order of 100 keV and 200 keV are respectively obtained for the 482 keV and 995 keV conversion electron peaks of ^{207}Bi .

3. Recoil ion Detectors

The Recoil Ion DETectors (RIDEs) of MORA are an adapted version of diagnostic detectors originally designed by LPC Caen for the SPIRAL 2 facility at GANIL. They consist of a stack of two large 5 x 5 cm MCPs from Photonis in chevron configuration, followed by a resistive anode imprinted on a flex PCB. A 90% transmission mesh at ground potential is placed 1 cm away from the front side of the MCP stack, which is biased at -4 kV. This configuration enables an electrostatic acceleration of ions for a maximal detection efficiency, while minimizing the disturbance of the recoil trajectories (see Fig. 2 of ref. [22] for further details). The resistive anode collects and splits the total charge resulting from the amplification of the initial signal into 4 localization charges. The position-sensitive flex consists of horizontal strips (pitch 1.3 mm) connected to their neighbors by means of a 10 Ω resistor. In and between the strips, pads (pitch 0.9 mm) are vertically connected on the back side of the Kapton PCB. Each vertical pad is also connected to its neighbors using 10 Ω resistors. The initial characterization of the RIDEs was done off-line at GANIL using a 3- α and an alkali ion source delivering $^{23}\text{Na}^+$ ions at a maximum energy of 1 keV, on a dedicated test bench. A stainless steel mask with regular holes of 1 mm diameter every 5 mm was used for position calibration (Fig. 16). The results of these tests were detailed in [22] and are briefly summarized here.

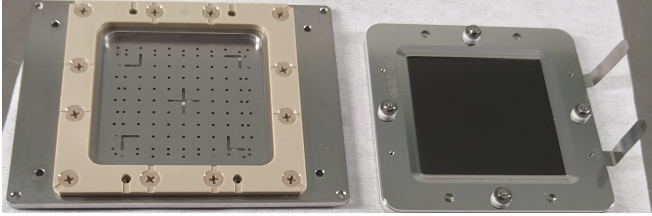


FIG. 16: Mask (left pane) and MCP stack (right pane) of one of the recoil ion detector of MORA.

The four charges enable reconstruction of the image using first order estimators for the x and y positions

$$\tilde{x} = \frac{Q_{right} - Q_{left}}{Q_{right} + Q_{left}} \quad (5)$$

$$\tilde{y} = \frac{Q_{top} - Q_{bottom}}{Q_{top} + Q_{bottom}} \quad (6)$$

where Q_{left} , Q_{right} , Q_{top} , Q_{bottom} correspond to the distributed charges collected on each side of the flex. The first order estimators yield an image as illustrated in the left pane of Fig. 17. The \tilde{x} and \tilde{y} values shown are dimensionless quantities, that can theoretically range from -1 and 1. In practice, they span a narrower range, from approximately -0.6 to 0.6, intentionally limited by a specific resistor configuration designed to balance the charges and

reduce possible threshold issues for detecting the smallest signals. This raw image is further transformed using polynomials of \tilde{x} and \tilde{y} up to the third order, to correct for aberrations mainly caused by screws maintaining the MCP stack, bringing the front voltage to the back of the stack [22]. The resulting image is shown on the right pane of Fig. 17. The collection of charges on a larger area than

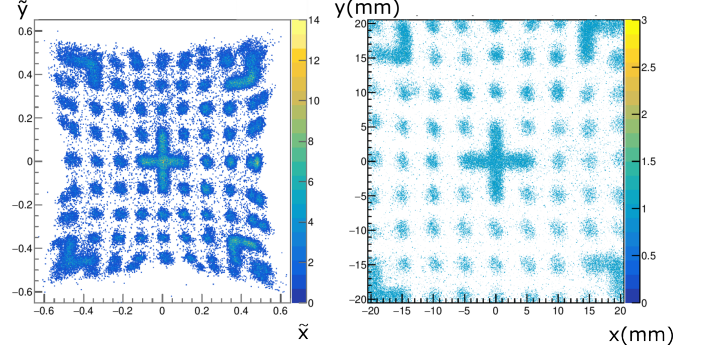


FIG. 17: Left pane: detector raw image showing the \tilde{x} and \tilde{y} estimators, constructed using the four localization charges coming from the position sensitive anode. Right pane: corrected image using polynomial forms of \tilde{x} and \tilde{y} up to the third order.

one strip or pad enables a barycentric reconstruction, resulting in a slightly enhanced spatial resolution compared to the pitch size between pads and strips of the anode. The resolution was determined using the cross in the center of the calibration mask with a side length of 5 mm. A projection of one side of the cross is illustrated in Fig. 18. It can be well reproduced by a step function convoluted by a normal law, i.e. an error function

$$F(y) = a \times \left(1 - \text{Erfc} \left(\frac{y - \mu_1}{\sqrt{2}\sigma_1} \right) \right) \quad (7)$$

where a and σ are a normalization factor and the gaussian smearing width due to the finite resolution of the anode, respectively and μ corresponds to the position of the falling/rising edge. In the fit, a and σ are left as free parameters whereas μ is fixed. Using this method, a resolution of 0.9 ± 0.4 mm in x and y is found in the center part of the detector image. On average, a position accuracy of better than 80 μm is achieved over the whole image after the third order reconstruction.

The absolute detection efficiency of the RIDE detectors for low energy $^{23}\text{Na}^+$ ions was additionally determined experimentally thanks to the off-line surface ionization source. In order to protect the MCPs from too high counting rates, a pA range (equivalently $\sim 10^7$ pps) beam was chopped thanks to a pulsed kicker voltage applied to a steerer of the ion source, and further attenuated by a 10% transmission mesh placed for the purpose in front of the detector. Such chopping technique produced pulses containing 1 or 2 ions over 2 μs every 10 ms. The intensity of the beam, when not chopped, was sufficient to

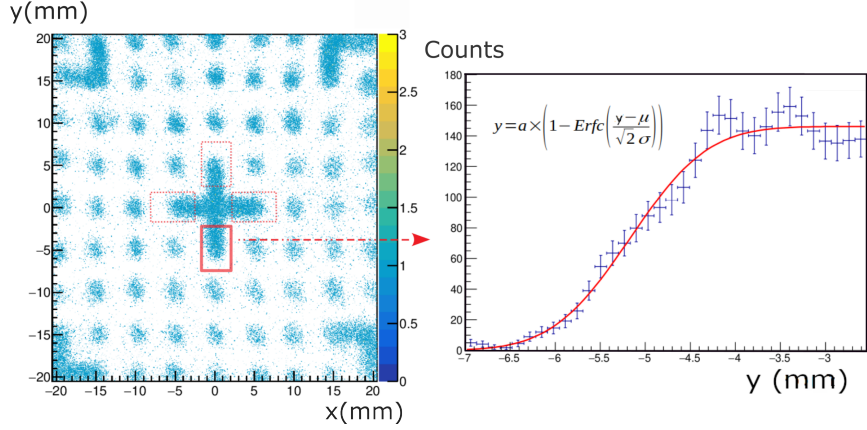


FIG. 18: Graphical cut of a 4.55 mm portion of the calibration cross on all four sides. In the right inset, the spectrum projected in the y plane fitted with an error function. See text for details.

allow for a direct measurement on the attenuation mesh with a picoammeter, with a precision of the order of 5 %. The absolute detector efficiency, η , was calculated taking into account different parameters using the following equation:

$$\eta = \frac{e \cdot (N_{ions} - N_{bgd})}{u \cdot I_{avg} \cdot \mu_{att}} \quad (8)$$

where N_{ions} corresponds to the number of counts integrated over the measurement time, N_{bgd} is the same number integrated over the same duration but in the absence of ions (kicker voltage always on), I_{avg} is the average current on the attenuation mesh measured before and after the measurement without kicker voltage, e is the electric charge, u is the duty cycle corresponding to the ratio between the chopping window and the cycle duration, and μ_{att} is the attenuation factor (~ 0.1) of the mesh in front of the MCP stack. The dependence of the efficiency on the acceleration voltage, obtained by biasing the front of the MCP stack at different voltages while adapting the voltage at the back to keep the same amplification factor is shown in Fig. 19. Error bars shown on this figure are only taking into account current variations observed on the continuous beam delivered by the ion source. Additional sources of uncertainty have to be taken into account. In particular the attenuation factor of the mesh is not known with a precision better than $\sim 10\%$, because of shadowing effects affecting the overall transmission of the $^{23}\text{Na}^+$ beam to the detector. These effects depend strongly on the focusing conditions of the ion beam, as was observed when setting up the test bench. The efficiency saturates for energies larger than 2.5 keV to a maximum value close to 50%, consistent with e.g. that obtained for the LPCTrap experiment [23].

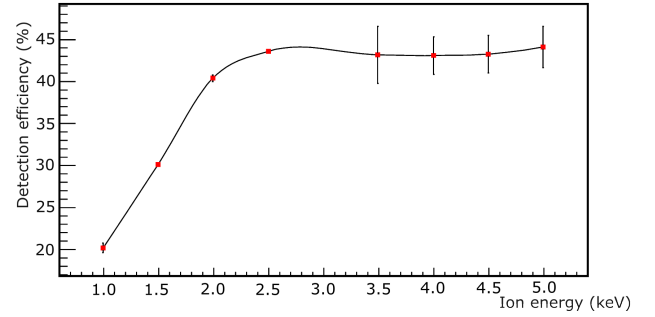


FIG. 19: RIDE detector efficiency as a function of the energy of the incoming ions.

III. SIMULATIONS

As introduced in section II E, the D correlation is inferred from an asymmetry of events involving β 's and recoil ions detected in coincidence at opposite angles, i.e. clockwise and anti-clockwise with respect to the spin of the nuclei (Fig. 10). Simulations have been undertaken to evaluate the sensitivity factor δ of Eq. 1 with better precision than in the first exploratory work [4], and to estimate the order of magnitude of possible systematic effects related to various experimental parameters, particularly those giving rise to dominant effects in the emiT experiment [7]. The Monte Carlo (MC) simulations developed in the framework of MORA are modular:

- The β decay of the $^{23}\text{Mg}^+$ ions in the trap is generated by a homemade code developed using the CERN ROOT libraries [24], providing the possibility to incorporate a realistic phase space for ions trapped and undergoing random collisions with a bath of ^4He atoms at $\simeq 300$ K.
- The resulting β decay phase space is then transferred to other transport codes for the tracking of positrons and recoil ions. For the positrons,

the PENELOPE MC code [25] is primarily used, sometimes in conjunction with GEANT 4 [26]. For recoil ions, SIMION [16] is employed.

A first estimate of the sensitivity factor α , appearing in Eq. 4 is also discussed below as it is used in the experimental determination of the polarization degree described in section IV.

A. Sensitivity factors

1. Sensitivity to the D correlation: δ

Given the transition of interest, the sensitivity parameter δ in Eq. 1 primarily depends on the phase-space coverage, which is determined by detection thresholds and solid angles of the detector. It is also expected to be affected by second-order instrumental effects, which include β scattering, the finite phase space volume of the trapped ion cloud, and the RF disturbance of recoil ion trajectories. These effects were neglected in a first approximation in [11] when determining δ for the decay of $^{23}\text{Mg}^+$ ions in the trap of MORA. To probe the dependence of δ on the first two effects, δ has been re-evaluated thanks to the aforementioned MC simulations, for the same detection solid angle as in [4] but this time taking into account β scattering using PENELOPE, and a Gaussian phase space for the ion cloud as derived for the analytical model described in [11]. Based on the actual RF, trap, and buffer gas settings, the ion cloud size is estimated as $\sigma_r = 2 \times \sigma_z \simeq 1.4$ mm, where σ_r and σ_z are the standard deviations of the cylindrical r and z positions of $^{23}\text{Mg}^+$ ions cooled by collisions with helium inside the trap. An effective temperature of $\simeq 730$ K, accounting for the so-called RF heating effect, was adopted to generate the velocity distribution (Eq. 31 of ref. [11]). The resulting δ is 0.765(1), which is less than 2% smaller than the previously determined value 0.775(1)[11]. The dilution in sensitivity to D caused by these two effects is rather small, as was anticipated in [4].

The study of the effect of the RF disturbance on the trajectory of recoil ions is ongoing. Preliminary results show that recoil directions are only marginally disturbed: the $\theta_{\beta r}$ angle between the β particle and the recoil ion directions is modified by less than 3° for 99.9% of the ions. An overall standard deviation of 0.9° for the $\theta_{\beta r}$ angle modifications is calculated. The loss in sensitivity to D caused by the RF disturbance is therefore expected to be even smaller than for the two previously studied effects.

2. Sensitivity to the polarisation degree: α

For the purpose of the proof-of-principle of the polarization technique (section IV), the sensitivity factor α appearing in Eq. 4 was estimated taking into account an

updated detection geometry. The simulations included a gaussian cloud as used in the case of the δ parameter. A threshold in energy of 250 keV, matching the experimental value, was applied. Above this energy the RF disturbance of the positron trajectories can safely be neglected. The α factor depends not only on the solid angle coverage but also on the value of the β asymmetry [4], whose value in the SM can be derived from β decay data: $A_\beta = -0.5584 \pm 0.0017$ [27]. In these conditions, the value of α has been estimated to be $\alpha = 0.51 \pm 0.01$ for the outer rings of the Si detectors, where a conservative 2% uncertainty was adopted for the dilution effect due to β scattering, which remains to be evaluated by PENELOPE simulations and has been neglected here.

B. Systematic effects

An ideal experiment would allow the simple extraction of the D parameter from Eq. 1. In practice, systematic effects may contribute to generate a fake D signature. These fake contributions must be evaluated to obtain precise results on D . As the MORA experimental design is an emiT-like one, the emiT experiment already provides an excellent overview of the possible and most important systematic effects [7]. Theoretically, a number of potential systematic effects can be canceled out by using appropriate detector symmetry and reversing the nuclear spin direction. As for emiT, MORA aims at using a combination of asymmetries obtained on single pairs of positron and recoil ion detectors by regularly inverting the spin direction of the ion cloud. We have started to investigate various phenomena that are expected to contribute to the systematic uncertainty on the D parameter:

1. The size of the ion cloud
2. A displacement of the ion cloud
3. A possible transverse polarization
4. An inhomogeneous polarization
5. The RF disturbance of the recoil ion trajectories
6. Variable detector efficiencies and thresholds.

When considered individually, such phenomena are not expected to produce any systematic effects because of the symmetries of the trap and detection setup. This was verified by simulations for the size of the ion cloud and the transverse polarization. A D_{fake} value consistent with 0 was obtained when reconstructing coincidence pairs between the positrons and recoil ions for a size of the ion cloud varying between $\sigma_r=1$ to 30 mm (see Fig. 20). Similarly, a D_{fake} value consistent with 0 was also obtained for a full transverse polarization contained in the azimuthal plane of the trap instead of the Z-axis.

A non-canceled fake D correlation values arises from crossed effects, at higher order, associating two of the

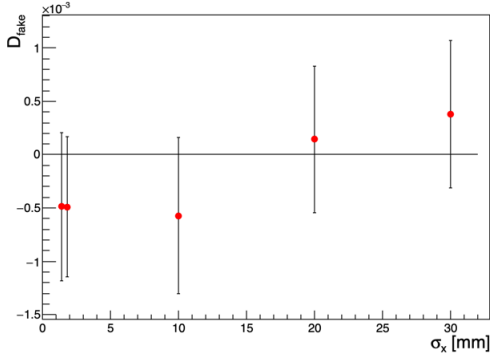


FIG. 20: Value of a potential fake D by varying the size of the ion cloud in the trap from $\sigma_x=1$ to 30 mm for a Gaussian-shaped cloud.

phenomena above. An example of such an effect, with its associated uncertainty dominating in the case of the emiT experiment [7], is the so-called asymmetric transverse polarization. The asymmetric transverse polarization results from a combination of a displacement of the decay vertices with respect to the detection setup and a transverse polarization. Such a combination of effects has been investigated for MORA, assuming in an extreme scenario that the ion cloud is displaced towards the x-axis by 5 mm along with a transverse polarization of 90° . As a result, the asymmetries do not cancel out, and a dummy value of D is found:

$$D_{fake} = 1.48 \times 10^{-4} \pm 1 \times 10^{-4}$$

The assumption of this scenario has been inflated on purpose, in order to obtain a sizable D_{fake} from the MC simulations. The mechanical tolerances, which have been used to build the MORA apparatus, allow for a maximum misalignment of the laser polarization direction of 1° to 2° , and for a maximal displacement of the ion cloud of the order of 1 mm. This would result in a maximal D_{fake} contribution of:

$$D_{fake} < 1 \times 10^{-6}.$$

Other effects will require a careful investigation, such as the ones associated with the disturbance of the recoil ions by the RF field, which are specific to MORA. In addition to the modification of their trajectory, the recoil ions can "see" their time-of-flight significantly altered, as shown in Fig. 21. Recording the RF phase at the time of the decay will allow to get a better event discrimination.

IV. FIRST EXPERIMENTAL RESULTS

A. Beam production and purification

At IGISOL, the $^{23}\text{Mg}^+$ ions are produced using a 30 MeV proton beam impinging on a thin target

of natural Mg through the most probable reaction $^{24}\text{Mg}(p,d)^{23}\text{Mg}$. Such a reaction has a cross section of about 140 mbarn according to the TALYS code [28]. Experimentally a yield of approximately $5 \cdot 10^5$ $^{23}\text{Mg}^+$ ions is obtained for 10 μA of primary beam, after production, stopping in the gas cell, transport through the sextupole ion guide (SPIG, see Fig. 1 and ref. [12]), and mass separation. During the first 2 years of MORA at IGISOL, a large contamination of the $^{23}\text{Mg}^+$ beam by a stable, isobaric beam of $^{23}\text{Na}^+$ prevented the measurement of the polarization degree [19, 29], which was the initial objective of the MORA campaigns at Jyväskylä. A current of $\gtrsim 100$ ppA of $^{23}\text{Na}^+$ ions has been consistently observed, dominating the $^{23}\text{Mg}^+$ yield by 3 orders of magnitude, while TALYS predicts a cross section with the associated nucleus only twice larger than for ^{23}Mg . Due to this contamination, only a limited number of $^{23}\text{Mg}^+$ ions could be transmitted by the minibuncher, which reaches saturation around 10^5 ions simultaneously trapped [13]. This resulted in only ~ 10 $^{23}\text{Mg}^+$ ions captured per cycle in the trap of MORA, when accounting for initial capture efficiencies around 10% (see section II C). Over these two years, a methodical investigation, reviewing the elements entering the production chain, finally permitted to identify a phenomenon of sputtering caused by He ions lost on the SPIG electrodes, as the main source of contamination. The contamination level could be drastically reduced in two recent beam times by:

- selecting a configuration of the gas purifier system to reduce the intensity of the He ion current lost on the SPIG electrodes (first beam time).
- tuning the parameters of the SPIG to trap and contain the sputtered $^{23}\text{Na}^+$ (first and second beam times).
- cleaning the SPIG electrodes using deionized water (second beam time).

In the first beam time, the tuning of the SPIG potentials and the injection of a He gas less purified than usual, bypassing a getter purifier, permitted to reduce the contamination ratio to a value $^{23}\text{Na}^+ : ^{23}\text{Mg}^+ \sim 10$, to the cost of a severe reduction of the $^{23}\text{Mg}^+$ yield, by 2 orders of magnitude. In the following beam time, the cleaning of the SPIG electrodes permitted to reduce the original contamination by a factor of approximately 10, from 100 ppA to $\simeq 10$ ppA without having to play with the settings of the SPIG, and without having to bypass the getter purifier. Unfortunately, several unfavorable factors diminished the anticipated benefit of contamination reduction. A modest yield of $6 \cdot 10^4$ $^{23}\text{Mg}^+$ per second at most was achieved, likely due to a combination of suboptimal proton beam tuning and a degraded target. The same tricks were used to contain the contamination in the SPIG, but this time achieving a more modest ratio of $^{23}\text{Na}^+ : ^{23}\text{Mg}^+ \sim 100$, likely because of an additional contamination from a neighboring beam ($^{22}\text{Ne}^+$ or molecule) that was not separated after the dipole magnet

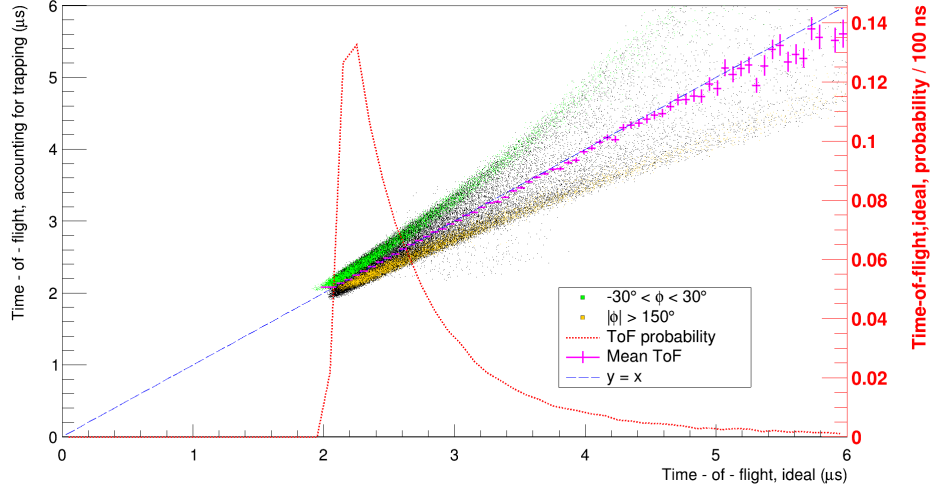


FIG. 21: Recoil ion Time-of-Flight (ToF) accounting for RF disturbance and finite ion cloud size effects, as simulated with SIMION. The x-axis shows the ToF of non-perturbed recoil ions while the y-axis on the left hand side shows the ToF including trapping effects. The simulation includes approximately 420,000 detected recoil ions, each represented by a dot. Recoil ions whose decays occur at extreme RF (ϕ) phases are plotted using different colors. The average ToF with respect to the RF phase (magenta markers) can be compared to the unperturbed case (dashed blue curve). The probability density of the ToF distribution is shown by a dashed red line and is referenced to the right-hand y-axis.

of IGISOL. As a result, the number of trapped ions was similar to that of the first beam time, despite an overall improvement in trapping efficiency (40% instead of 10% thanks to the stabilization of the PDT1, see section II C) and a lower contamination. Nevertheless, the longer acquisition time permitted to achieve the first measurement of the polarization degree, which is described thereafter.

B. Experimental demonstration of polarization

The reduction of the contamination level permitted for the first time:

- The recording of β - recoil ion coincidences.
- The consistent determination of the number of trapped ions from their observed radioactivity inside the trap.
- The determination of asymmetries for the $\sigma+$ and $\sigma-$ circular polarization of the laser light, even with a so-far modest precision. From these asymmetries a first estimate of the polarization degree could be obtained, as detailed below.

During the measurement time, cycles of 11 s duration, which nearly correspond to the $^{23}\text{Mg}^+$ half-life, were adopted. The cycles were divided into 6 s for trapping, and 5 s for background measurement after the ejection of the ion cloud to MCP2 (section II C). These cycles permitted to contain the accumulation of background from lost ions around the trap, near the Si detectors, for the determination of asymmetries.

1. β - recoil ion coincidences

Figure 22 shows the number of RIDE - phoswich detector coincidences as a function of the time elapsed between the detection of events. The phoswich detectors have one order of magnitude larger probability of detecting coincidences than Si detectors, because of a combination of larger solid angle and higher phase space probability in the β decay spectrum. During trapping the coincidence spectrum exhibits two peaks. The first one with $\delta t \simeq 0$, corresponds to β - β coincidences, with a possible contribution from RF-induced noise that may simultaneously trigger the detectors. The second, starting after 2 μs corresponds to the expected time-of-flight distribution of recoiling ions (see Fig. 21). A constant evaporation of $^{23}\text{Na}^+$ ions from the trap (Fig. 8) causes a higher overall background during the trapping period of the cycle. After the first peak, a slight increase in the coincidence rate can be observed both during the trapping period, and after the ejection of ions towards MCP2 (blue dashed curve). This slight increase is likely caused by the detection of ions, either a recoil ion, a helium ion, or a residual gas molecule ionized by the β particle emitted by a $^{23}\text{Mg}^+$ ion implanted near a RIDE or a phoswich detector.

2. Detection of the radioactivity of trapped ions on Si detectors

The annular Si1 and Si2 detectors described in section II E 1 are positioned with respect to the trap and

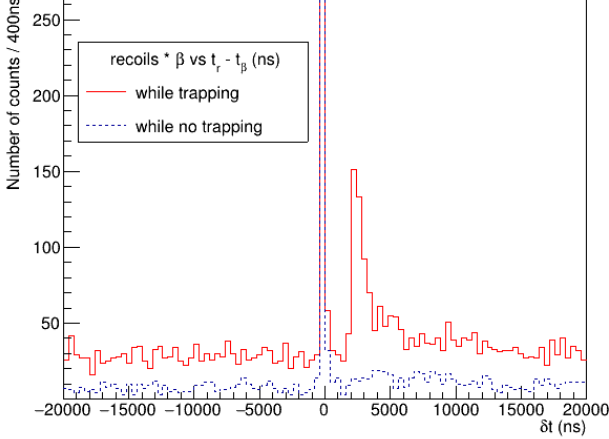


FIG. 22: Recorded coincidences. δt is the time difference between the detection of an event on a RIDE detector and of a β particle on a phoswich detector.

laser as shown in Fig. 2. Figure 23 shows the count rate of positrons detected over the cycle by the outer sectors (odd sectors in Fig. 12) of Si1 and Si2, during the illumination of the ion cloud with laser light with $\sigma+$ and $\sigma-$ circular polarization. A global threshold of 250 keV was applied to all Si sectors, to limit the contribution of RF-induced background. The data corresponds to 9 hours for each circular polarization, accumulated over successive 1-hour runs. The polarization was flipped between each successive runs. The excess of events observed during the trapping period is attributed to positrons emitted by trapped ions. The large, exponentially decaying background is caused by losses around the detectors during the injection and ejection of ions into/from the trap. Such a background is even more prominent on the inner sectors of the Si detectors (even sectors in Fig. 12), which are exposed to direct deposition of lost ions during these phases. They are excluded from the present analysis because of their much lower signal to noise ratio.

The dashed horizontal lines are fits of the environmental background, in the absence of injected ions, but with all switching pulses and RF on. The RF is being kept on during the whole cycle. As expected the environmental background shows no statistically significant modification following the ejection pulse, which occurs 6 s after the start of the cycle. The number of trapped ions whose decay has been detected by Si1 and Si2 are inferred from a global fit of the data. They are listed in Tab. I together with the two types of asymmetries introduced in section II E, proportional to the polarization degree (see section IV B 4).

3. Number of trapped ions

Estimates of the number of trapped ions in the cycle can be derived from the number of recorded coincidences and positrons detected by the Si detectors, taking into account the measured detector efficiencies, and using the results of a Monte Carlo simulation similar to the one discussed in section III A for the determination of the sensitivity factor α , updated to reflect the actual detection setup geometry. The results of this investigation shows consistent estimates for the number of trapped $^{23}\text{Mg}^+$ ions per cycle N_c :

- $N_c = 93 \pm 11$, from the number of positrons detected by the outer sectors of the Si1 and Si2 detectors and attributed to trapped ions.
- $N_c = 104 \pm 11$ from the number of recorded coincidences.

Such a number, $N_c \simeq 100$ ions per cycle, remains 2 orders of magnitude lower than the one aimed at for the measurement of the D correlation coefficient at IGISOL (see Tab. 2 of ref. [4]). Various ways to increase N_c are being investigated, including addressing the issues encountered during the last beam time, related to the suboptimal $^{23}\text{Mg}^+$ yield and separator tuning.

4. Polarization degree from asymmetries.

The two types of experimental asymmetries described in section II E (A^+ , A^- in Eq. 2 and A_1 , A_2 in Eq. 3) were derived from the analysis of the data shown in Fig. 23. They are displayed in Tab. I. They are equivalent under the assumptions that Si1 and Si2 detectors have similar efficiencies, and that the activity accumulated over the $\sigma-$ and $\sigma+$ laser light illumination periods is similar. In the present case, these assumptions are justified by the limited precision with which the asymmetries are determined: approximately 30%, to be compared to % level effects on the number of counts detected by Si1 and Si2. This is confirmed by the calculation of weighted averages of the absolute values of the asymmetries A^+ , A^- on the one hand, and A_1 , A_2 on the other. In the limit of their precision, the averages are identical, as anticipated. They are also found to be equal to the maximum allowed value by Eq. 4: $|\bar{A}| = 0.51 \pm 0.14$. The latter result can be transformed into a Confidence Level (CL) interval for the polarization degree: $0.55 < P < 1$ at 90 % CL, which is also - as a matter of fact - identical for both frequentist and Bayesian inferences. Even if the determination of experimental asymmetries is quite qualitative at this stage, it shows that, as expected, the polarization degree of ions trapped in MORA is large, most probably above 50%.

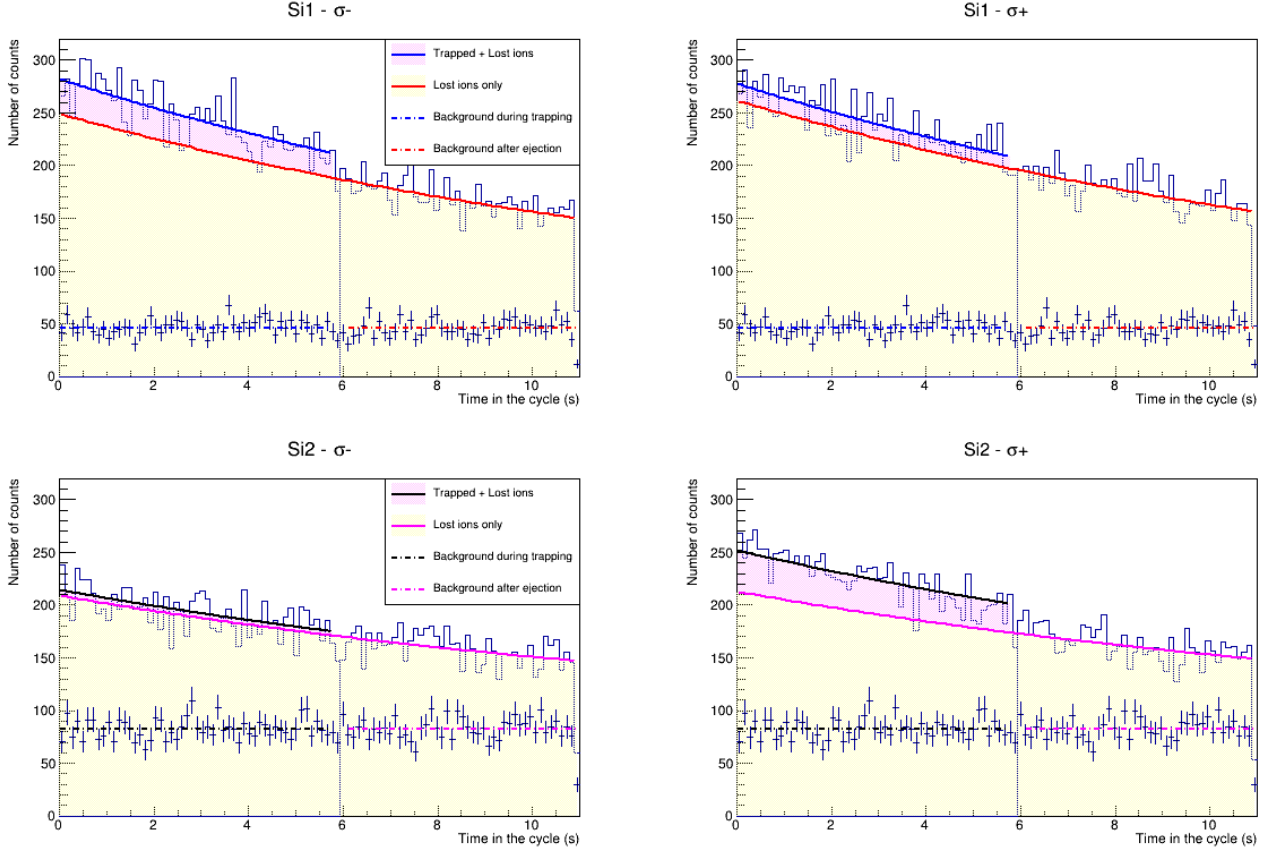


FIG. 23: Count rates as detected by the outer sectors of the Si1 and Si2 detectors over the cycle, for $\sigma-$ and $\sigma+$ circular laser polarization. See text for more details.

	Si1	Si2	A^+/A^-
$\sigma+$	720 ± 270	1750 ± 260	$A^+ = -0.42 \pm 0.16$
$\sigma-$	1480 ± 260	240 ± 250	$A^- = 0.72 \pm 0.25$
A_1/A_2	$A_1 = 0.35 \pm 0.18$	$A_2 = -0.76 \pm 0.22$	$ \bar{A} = 0.51 \pm 0.14$

TABLE I: Number of trapped ion decays detected in each Si detector as deduced from the global fit of Fig. 23, and corresponding asymmetries (Eq. 2 and 3).

V. CONCLUSION

The MORA apparatus has been undergoing an intense commissioning period at IGISOL, in the JYFL Accelerator Laboratory at the University of Jyväskylä. Trapping efficiencies around 40% have been obtained after the stabilization of the switching voltages of the main pulsed drift tube. $^{23}\text{Mg}^+$ ions can be trapped over times much larger than their radioactive half-life. The detection setup is operational. Nominal performances were achieved in terms of recoil-ion detection efficiency and positioning on MCP-based detectors, as well as β -energy resolution using segmented Si detectors and 4-quadrant phoswich scintillators. Nominal laser power, above 50 mW at 280 nm could be achieved during all the

test beam times. This power is more than sufficient to saturate the ionic transition in $^{23}\text{Mg}^+$. Recent progress on reducing the challenging issue of isobaric beam contamination permitted, for the first time, to record β -recoil ion coincidences, and to achieve the proof-of-principle of the innovative polarization technique. The measurement of the polarization degree remains at this stage quite qualitative, indicating a polarization degree above 55% at 90 % CL. More data will be acquired in the next months to enable a measurement with a precision better than 10 %, using both the detection of single positrons on the annular Si detectors and of coincidences between these positrons and recoil ions detected in the azimuthal plane of the trap. The current number of $^{23}\text{Mg}^+$ ions trapped per cycle is of the order of 100.

This number is still two orders of magnitude too low to initiate a D measurement in the decay of $^{23}\text{Mg}^+$ ions at the desired sensitivity level. Various improvements are under consideration, including the recovery of nominal $^{23}\text{Mg}^+$ yields from the IGISOL gas cell, with a careful proton beam tuning on target, and the suppression of non-isobar contamination by the fine adjustment of the optics of the dipole separator. The level of $^{23}\text{Na}^+$ contamination has been reduced by a factor of 10 by cleaning the surfaces of the SPIG electrodes. These electrodes, in stainless steel, are going to be exchanged with Nb rods, baked at high temperature ($> 1400^\circ\text{C}$) to eliminate in-depth Na impurities via their diffusion from the bulk material. Before MORA comes back to GANIL, future plans at IGISOL include in addition to the precision measurement of the D correlation in the decay of $^{23}\text{Mg}^+$ ions, the investigation of a measurement involving $^{39}\text{Ca}^+$ ions. Because of a $\sim 10\times$ shorter radioactive half-life, $^{39}\text{Ca}^+$ ions potentially enable a measurement with even superior sensitivity to New Physics than $^{23}\text{Mg}^+$ ions. A $^{39}\text{Ca}^+$ beam will a priori not be free of impurities as a large current of $^{39}\text{K}^+$ ions, at least as large as the one of $^{23}\text{Na}^+$, of the order of 100 ppA, was observed from the gas cell used for the $^{23}\text{Mg}^+$ beam production. Prospects are therefore also ongoing for developing an universal purification scheme at IGISOL, making use of a stacking trap to accumulate clean and intense $^{23}\text{Mg}^+$ and $^{39}\text{Ca}^+$ bunches after fast, ~ 10 ms cycles in the MR-ToF-MS. In parallel, investigations have been starting at GANIL for the production of an intense $^{39}\text{Ca}^+$ beam from the SPIRAL 1 facility to prepare future campaigns of the MORA experiment at the DESIR facility, which is presently under development. The experimental activities are accompanied by the development of a simulation framework to prepare for high sensitivity measurements. This framework, combining homemade codes, PENELOPE, GEANT 4 and SIMION, enables a

detailed study of sensitivity factors and a comprehensive investigation of potential systematic effects that could impact the results of a precise D correlation measurement. The precise determination of sensitivity factors to the polarization degree, on one hand, and to the beta asymmetry, on the other, is being carried out by incorporating all relevant experimental parameters into the simulation. The largest systematic effects studied so far, dominant in the case of the emiT experiment, are not expected to limit a D correlation measurement at the 10^{-5} level. Current efforts focus on studying effects related to RF disturbances affecting the ToF of recoil ions traveling to their detectors, which are specific to MORA.

ACKNOWLEDGMENTS

This project has received funding from Région Normandie, the Agence Nationale de la Recherche (ANR) under contract ANR-19-CE31-0012-01. Mobility has funds have been provided from the ACCLAB-GANIL bilateral agreement, and the European Union's Horizon Europe Research and Innovation Programme under Grant Agreement No. 101057511 (EURO-LABS).

Authors of this paper have received fundings from the Research Council of Finland projects No. 295207, No. 327629, No. 306980, No. 354589 and No. 354968, and from the FWO Research Foundation-Flanders' International Research Initiatives projects I002219N and I001323. The work of authors from IFIC has been supported by MCIN/AEI/10.13039/501100011033 (grants PID2020-114473GB-I00 and PID2023-146220NB-I00), by CIDEIG/2023/12, by MICIU/AEI/10.13039/501100011033 and European Union NextGenerationEU/PRTR (grant CNS2022-135595).

-
- [1] M. González-Alonso and O. Naviliat-Cuncic, “Prospects for precision measurements in nuclear beta decay at the lhc era,” (2013).
 - [2] M. González-Alonso, O. Naviliat-Cuncic, and N. Severijns, *Progress in Particle and Nuclear Physics* **104**, 165 (2019).
 - [3] A. Falkowski, M. González-Alonso, and O. Naviliat-Cuncic, *Journal of High Energy Physics* **2021**, 126 (2021).
 - [4] P. Delahaye, E. Liénard, I. Moore, M. Benali, M. L. Bissell, L. Canete, T. Eronen, A. Falkowski, X. Fléchar, M. Gonzalez-Alonso, W. Gins, R. P. D. Groote, A. Jokinen, A. Kankainen, M. Kowalska, N. Lecesne, R. Leroy, Y. Merrer, G. Neyens, F. D. O. Santos, G. Quemener, A. D. Roubin, B.-M. Retaillieu, T. Roger, N. Severijns, J. C. Thomas, K. Turzo, and P. Ujic, *Hyperfine Interactions* **240** (2019), 10.1007/s10751-019-1611-x.
 - [5] A. D. Sakharov, *Soviet Physics Uspekhi* **34**, 392 (1991).
 - [6] A. Falkowski and A. Rodríguez-Sánchez, *The European Physical Journal C* **82**, 1134 (2022).
 - [7] T. E. Chupp, R. L. Cooper, K. P. Coulter, S. J. Freedman, B. K. Fujikawa, A. García, G. L. Jones, H. P. Mumm, J. S. Nico, A. K. Thompson, C. A. Trull, F. E. Wietfeldt, and J. F. Wilkerson, *Physical Review C* **86**, 035505 (2012).
 - [8] H. P. Mumm, T. E. Chupp, R. L. Cooper, K. P. Coulter, S. J. Freedman, B. K. Fujikawa, A. García, G. L. Jones, J. S. Nico, A. K. Thompson, C. A. Trull, J. F. Wilkerson, and F. E. Wietfeldt, *Physical Review Letters* **107**, 102301 (2011).
 - [9] J. Äystö, T. Eronen, A. Jokinen, A. Kankainen, I. D. Moore, and H. Penttilä, eds., *IGISOL. Three decades of research using IGISOL technique at the University of Jyväskylä* (Springer, Berlin, Germany, 2014).
 - [10] M. Benali, G. Quémener, P. Delahaye, X. Fléchar, E. Liénard, and B. M. Retaillieu, *The European Physi-*

- cal Journal A **56**, 163 (2020).
- [11] P. Delahaye, The European Physical Journal A **55** (2019), 10.1140/epja/i2019-12740-4.
 - [12] P. Karvonen, I. Moore, T. Sonoda, T. Kessler, H. Penttilä, K. Peräjärvi, P. Ronkanen, and J. Äystö, Nuclear Instruments and Methods in Physics Research Section B: Beam Interactions with Materials and Atoms **266**, 4794 (2008).
 - [13] V. Virtanen, T. Eronen, A. Kankainen, O. Beliuskina, P. Campbell, R. Delaplanche, Z. Ge, R. de Groote, M. Hukkanen, A. Jaries, R. Kronholm, I. Moore, A. Raggio, A. de Roubin, J. Ruotsalainen, and M. Schuh, Nuclear Instruments and Methods in Physics Research Section A: Accelerators, Spectrometers, Detectors and Associated Equipment **1072**, 170186 (2025).
 - [14] T. Eronen, V. Kolhinen, V.-V. Elomaa, D. Gorelov, U. Hager, J. Hakala, A. Jokinen, A. Kankainen, P. Karvonen, S. Kopecky, I. D. Moore, H. Penttilä, S. Rahaman, S. Rinta-Antila, J. Rissanen, A. Saastamoinen, J. Szerypo, C. Weber, and J. Äystö, Eur. Phys. J. A **48**, 46 (2012).
 - [15] S. Kujanpää, A. Raggio, R. de Groote, M. Athanasakis-Kaklamanakis, M. Block, A. Candiello, W. Gins, A. Koszorús, I. Moore, M. Reponen, and J. Warbinek, Nuclear Instruments and Methods in Physics Research Section B: Beam Interactions with Materials and Atoms **541**, 388 (2023).
 - [16] D. McGilvery and D. Dahl, <https://simion.com>.
 - [17] faster@lpccaen.in2p3.fr, “Faster web site,” (2025), <https://faster.in2p3.fr/> [Accessed: (2025/04/09)].
 - [18] R. E. March and J. F. J. Todd, “Theory of quadrupole instruments,” in *Quadrupole Ion Trap Mass Spectrometry* (John Wiley & Sons, Ltd, 2005) Chap. 2, pp. 34–72.
 - [19] S. Daumas Tschopp, *Search for CP violation with MORA: commissioning of the setups and first experiments*, Ph.D. thesis, Université de Caen Normandie (2023), thèse de doctorat dirigée par Liénard, Etienne Physique Normandie 2023.
 - [20] B. Pons, Private Communication (2022).
 - [21] R. Rispoli, E. De Angelis, L. Colasanti, N. Vertolli, S. Orsini, J. Scheer, A. Mura, A. Milillo, P. Wurz, S. Selci, *et al.*, in *Modern Technologies in Space-and Ground-based Telescopes and Instrumentation II*, Vol. 8450 (SPIE, 2012) pp. 1792–1798.
 - [22] N. Goyal, S. Daumas-Tschopp, F. De Oliveira Santos, P. Delahaye, X. Flechard, J. M. Fontbonne, E. Lienard, L. M. Motilla, J. Perronnel, G. Quemener, and A. Singh, Journal of Physics: Conference Series **2586**, 012142 (2023).
 - [23] E. Liénard, M. Herbane, G. Ban, G. Darius, P. Delahaye, D. Durand, X. Fléchar, M. Labalme, F. Mauger, A. Mery, O. Naviliat-Cuncic, and D. Rodríguez, Nuclear Instruments and Methods in Physics Research Section A: Accelerators, Spectrometers, Detectors and Associated Equipment **551**, 375 (2005).
 - [24] I. Antcheva, M. Ballintijn, B. Bellenot, M. Biskup, R. Brun, N. Buncic, P. Canal, D. Casadei, O. Couet, V. Fine, L. Franco, G. Ganis, A. Gheata, D. G. Maline, M. Goto, J. Iwaszkiewicz, A. Kreshuk, D. M. Segura, R. Maunder, L. Moneta, A. Naumann, E. Offermann, V. Onuchin, S. Panacek, F. Rademakers, P. Russo, and M. Tadel, Computer Physics Communications **180**, 2499 (2009), 40 YEARS OF CPC: A celebratory issue focused on quality software for high performance, grid and novel computing architectures.
 - [25] A. E. Salvat F., Fernandez-Varea J.M. and J. Sempau, Nuclear Energy Agency of the OECD (NEA) (2015).
 - [26] S. Agostinelli, J. Allison, K. Amako, J. Apostolakis, H. Araujo, P. Arce, M. Asai, D. Axen, S. Banerjee, G. Barrand, F. Behner, L. Bellagamba, J. Boudreau, L. Broglia, A. Brunengo, *et al.*, Nuclear Instruments and Methods in Physics Research Section A: Accelerators, Spectrometers, Detectors and Associated Equipment **506**, 250 (2003).
 - [27] N. Severijns, M. Tandecski, T. Phalet, and I. S. Towner, Physical Review C **78**, 055501 (2008).
 - [28] Koning, Arjan, Hilaire, Stephane, and Goriely, Stephane, Eur. Phys. J. A **59**, 131 (2023).
 - [29] N. Goyal, *Detection of beta decay in laser oriented trapped radioactive isotopes for the MORA project*, Ph.D. thesis, Université de Caen Normandie (2023), thèse de doctorat dirigée par De Oliveira Santos, François Physique Normandie 2023.